



HAL
open science

Molecular interaction of fibrinogen with zeolite nanoparticles

Hossein Derakhshankhah, Atiyeh Hosseini, Fereshteh Taghavi, Samira Jafari, Alireza Lotfabadi, Mohammad Reza Ejtehadi, Sahba Shahbazi, Ali Fattahi, Atiyeh Ghasemi, Ebrahim Barzegari, et al.

► **To cite this version:**

Hossein Derakhshankhah, Atiyeh Hosseini, Fereshteh Taghavi, Samira Jafari, Alireza Lotfabadi, et al.. Molecular interaction of fibrinogen with zeolite nanoparticles. Scientific Reports, 2019, 9 (1), pp.1558. 10.1038/s41598-018-37621-4 . hal-02047597

HAL Id: hal-02047597

<https://normandie-univ.hal.science/hal-02047597>

Submitted on 1 Dec 2020

HAL is a multi-disciplinary open access archive for the deposit and dissemination of scientific research documents, whether they are published or not. The documents may come from teaching and research institutions in France or abroad, or from public or private research centers.

L'archive ouverte pluridisciplinaire **HAL**, est destinée au dépôt et à la diffusion de documents scientifiques de niveau recherche, publiés ou non, émanant des établissements d'enseignement et de recherche français ou étrangers, des laboratoires publics ou privés.



Distributed under a Creative Commons Attribution 4.0 International License

Molecular interaction of fibrinogen with zeolite nanoparticles

Hossein Derakhshankhah,^{a,b,c,d,g} Mohammad Javad Hajipour,^{e,f} Fereshteh Taghavi,^g Alireza Lotfabadi,^{b,c,d} Atiyeh Ghasemi,^g Ebrahim Barzegari,^g Mina Evini,^g Ali Akbar Saboury,^g Eng-Poh Ng,^h Seyed Mehdi Kamali Shahri,ⁱ Hussein Awala,^j Svetlana Mintova,^{*j} Rassoul Dinarvand^{*b,c} and Morteza Mahmoudi,^{*b,c,k}

^a Department of Pharmaceutical Biomaterials, Faculty of Pharmacy, Kermanshah University of Medical Sciences, Kermanshah, Iran.

^b Nanotechnology Research Center, Faculty of Pharmacy, Tehran University of Medical Sciences, Tehran 13169-43551, Iran.

^c Department of Pharmaceutical Nanotechnology, Faculty of Pharmacy, Tehran University of Medical Sciences, Tehran 13169-43551, Iran.

^d Department of Pharmaceutical Biomaterials, Faculty of Pharmacy, Tehran University of Medical Sciences, Tehran 13169-43551, Iran.

^e Persian Gulf Marine Biotechnology Research Center, The Persian Gulf Biomedical Sciences Research Institute, Bushehr University of Medical Sciences, Bushehr 75147, Iran.

^f Non-Communicable Diseases Research Center, Endocrinology and Metabolism Population Sciences Institute, Tehran University of Medical Sciences, Tehran 13169-43551, Iran.

^g Institute of Biochemistry and Biophysics, University of Tehran, Tehran, Iran.

^h School of Chemical Sciences, Universiti Sains Malaysia, 11800 USM, Malaysia.

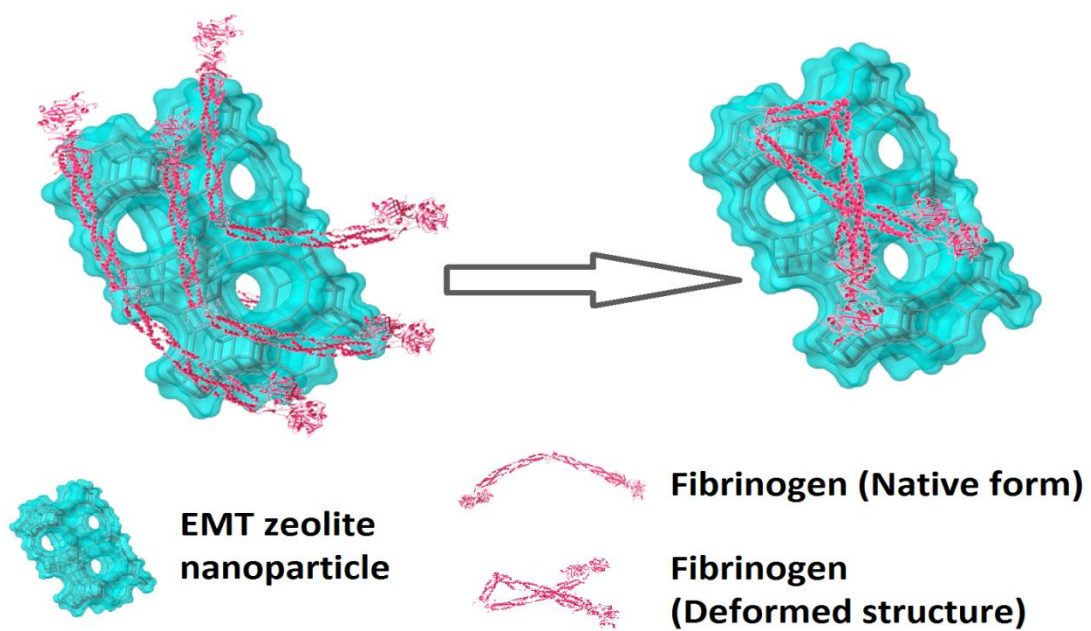
ⁱ Department of Chemical Engineering, The Pennsylvania State University, University Park, PA 16802, United States.

^j Laboratory of Catalysis and Spectroscopy, ENSICAEN, University of Caen, CNRS, 6 Boulevard du Marechal Juin, 14050 Caen, France.

^k Department of Anesthesiology, Brigham and Women's Hospital, Harvard Medical School, Boston, Massachusetts 02115, United States.

* Corresponding authors: (RD) email: dinarvand@tums.ac.ir; (SM) email: mintova@ensicaen.fr; (MM) email: mmahmoudi@bwh.harvard.edu

TOC



Abstract

Physicochemical properties of nanoparticles direct the way proteins bind to their surfaces and make a protein-based layer. Parameters such as the type, quantity, and conformation of the participated proteins in the protein layer (i.e., protein corona) affect the response of biological systems. Fibrinogen is one of the key proteins that participate in the protein corona composition of many types of NPs, and its conformational changes are crucial for activation of immune systems. Recently, we demonstrated the fibrinogen highly contributed in the protein corona composition at the surface of zeolite nanoparticles. Therefore, understanding the interaction of fibrinogen with zeolite nanoparticles in more details could shed light of their safe applications in medicine. Thus we probed the molecular interactions between fibrinogen and zeolite nanoparticles using several experimental approaches including fluorescence, UV-visible spectroscopy, and circular dichroism (CD) spectroscopy. The results indicated that fibrinogen has strong and thermodynamically favorable interaction with zeolite nanoparticles in a non-cooperative manner. Additionally, fibrinogen experienced a substantial conformational change in the presence of zeolite nanoparticles through concentration-dependent manner.

Keywords: Zeolite nanoparticles; Fibrinogen; Conformational change; Protein-nanoparticles interactions.

Introduction

Nanoparticles (NPs) surfaces are instantaneously covered by a layer of biomolecules (so-called protein corona), when they come into contact with physiological fluids such as blood plasma¹⁻⁴. The competitive adsorption of proteins on the NP surface is dependent on the physicochemical properties of NPs, incubation condition (time and temperature), and plasma protein alterations (protein concentration/structure) mediated by diseases⁴⁻¹⁰. In fact, the formation of protein corona changes the surface properties of NPs and it provides a biological mask, which is being “seen” by the biological systems such as cells^{2, 11-15}. The type, concentration and configuration of the participated proteins in the corona layer can give useful information for predicting the biological fate of NPs including their pharmacokinetics and biodistribution^{5, 9, 16-19}.

During last few years, many studies were devoted on achieving in-depth information on the structural integrity of proteins after participating in the corona structure; As expected, the preliminary results revealed that the degree of structural rearrangement in protein is dependent on the protein type and physicochemical properties of NPs.^{9, 20, 21}. As an example of the role of protein type, fibrinogen demonstrated higher structural changes compared to albumin when interacting with graphene oxide⁹ and silica NPs²¹. Regarding the NPs’ properties, hydrophobic surfaces induce more structural changes to both albumin and fibrinogen compared to hydrophilic surfaces²¹.

Moreover, the structural variations of proteins can change their physiological functions. For example, we demonstrated that transferrin experiences irreversible structural changes and loose the main functionality (i.e., transport of iron among cells) after adsorption to the surface of iron

oxide NPs²². Along with the functional changes, the structural changes in some proteins may activate inflammatory responses. For instance, structural changes in fibrinogen (i.e., exposure of its C-terminous of γ chain ($\gamma^{377-395}$)), after interaction with poly(acrylic acid)-coated gold NPs, can provoke the inflammation response and downstream unwanted cascade pathways¹⁸.

The structural changes in proteins, after participating in the corona layer, can affect the cellular uptake mechanism of nanoparticles. For example, bovine serum albumin (BSA) proteins adsorbed on the surface of cationic polystyrene NPs experienced structural changes, while the bounds to anionic polystyrene remained intact²³. These variations in the protein structure at the corona layer led to different interactions of the NPs with the cell receptors, i.e. the BSA-coated cationic and anionic NPs bounded to scavenger and native albumin receptors, respectively. In a similar study, Minchin group²⁴ demonstrated that the silica NPs have capability to change the albumin's structure, leading to exposure of a typical hidden epitope, which is exclusively recognized by macrophages expressing class A receptor. Prapainop *et al.*²⁵ demonstrated that apolipoprotein conformational was changed after binding to quantum dots and it substantially increased their uptakes by macrophages. Thus the challenges associated with the structural integrity of corona proteins raised serious concerns about the *in vivo* fate/behavior of NPs.

Zeolite NPs have promising potential medical applications including drug delivery, imaging, and microbial infection and neurodegenerative diseases therapy²⁶⁻²⁹. Probing the structure of adsorbed proteins on the surface of zeolite NPs is of great interest as it helps scientists in the field to maximize the therapeutic efficacy of these particles while maintaining the toxic effects at minimal level. Recently, we demonstrated that fibrinogen has the most contribution, among other plasma proteins, in the corona structure of the zeolite NPs^{30, 31}. However, the molecular interactions between zeolite NPs and fibrinogen are inadequately understood. The aim of this

work is to understand the nature of interaction of zeolite nanoparticles with fibrinogen through probing the binding kinetics, thermodynamic parameters and structural changes using a wide range of experimental approaches including fluorescence and UV-visible spectroscopy, and circular dichroism (CD) spectroscopy.

Experimental Section

Synthesis and characterization of EMT zeolite NPs

The EMT NPs were synthesized as follows:³² Aluminate solution was prepared by mixing 9.07 g of sodium aluminate (Strem Chemicals), 1.61 g of sodium hydroxide (Prolabo, 97%) and 100.00 g of double distilled water. The mixture was stirred for 10 min before another 44.00 g of sodium hydroxide was added to the solution. The solution was continuously stirred until a resulting clear aluminate suspension was obtained. The silicate solution was prepared by dissolving 57.69 g of sodium silicate (Prolabo, 27% SiO₂, 8% Na₂O) and 20.00 g of sodium hydroxide in 80.00 g of double distilled water. The preparation of both solutions involved exothermic reaction and hence both solutions should be cooled down in an ice bath (4 °C). The aluminate solution was then slowly poured into the silicate solution under magnetic stirring (800 rpm); a white colloidal suspension with a molar composition of 1Al₂O₃:5.15SiO₂:18.45Na₂O:240H₂O was obtained. The resulting suspension was stirred for additional 5 min before it was crystallized at 30 °C for 36 h under static condition. The resulting EMT zeolite nanocrystals were then centrifuged (20000 rpm for 1 h) and purified with distilled water until the pH of the suspension reached 7.

The XRD patterns of zeolite NPs were obtained using a PANalytical X'Pert PRO XRD diffractometer (step size 0.01°, 1.5 seconds per step, Cu-K_α radiation). The morphology and crystallite size of zeolite samples were inspected by a transmission electron microscope (TEM) (JEOL Model 2010 FEG system, 200 kV). The average size of zeolite NPs was determined by randomly counting 50 particles through TEM observations obtained in different regions. The hydrodynamic size and zeta potential, ζ , of colloidal solution of zeolite NPs (1 wt%, pH 7.5, 25 °C) were measured by a Malvern Zetasizer Nano Series equipment. The surface charge density, σ , was calculated using the Grahame equation (Eq. 1):

$$\sigma = \sqrt{8c_0 \epsilon \epsilon_0 k_B N_A T} \times \sinh\left(\frac{e\Psi_0}{2k_B T}\right) \quad (\text{Eq. 1})$$

where c_0 is the concentration of zeolite (0.1%) in suspension in unit m^3 , $\epsilon\epsilon_0$ is the dielectric permittivity of EMT zeolite ($1.3547 \times 10^{-11} \text{ AsV}^{-1} \text{ m}^{-1}$), k_B is the Boltzmann constant ($1.381 \times 10^{-23} \text{ J K}^{-1}$), Ψ_0 is the surface potential or zeta potential of the zeolite suspension (-45.7 mV), e is the electronic charge ($1.602 \times 10^{-19} \text{ C}$), and T is the absolute temperature (298 K).

The surface charge of EMT NPs, Q , was computed by using Eq. 2:

$$Q = \frac{\sigma \times S_{\text{BET}}}{\text{Si / Al ratio}} \quad (\text{Eq. 2})$$

where S_{BET} is the specific surface area ($\text{m}^2 \text{ g}^{-1}$) and Si/Al ratio is the silicon to aluminum ratio of the zeolite NPs.

The elemental analysis was characterized by using a Phillips X'Unique X-ray Fluorescence (XRF) spectrometer. The porosity of zeolite NPs was analyzed by a Micromeritics ASAP 2010 nitrogen adsorption analyzer. Prior to analysis, the powder was dehydrated at $250 \text{ }^\circ\text{C}$ under vacuum overnight. The specific surface area was calculated using the BET equation while the external surface area and micropore volume were computed using the t -plot technique. The pore sizes were calculated using the Density Functional Theory (DFT) model provided by Micromeritics software.

Fluorescence spectroscopy

Fluorescence quenching of fibrinogen was measured in the presence of increasing concentrations of zeolite NPs using spectrofluorometer (Hitachi MPF-4, equipped with a thermostatically

controlled cuvette compartment). The fluorescent property of fibrinogen is related to its aromatic amino acids such as tryptophan (Excitation: 280 nm; Emission: 360 nm). This analysis was performed at different temperatures (25, 37, 40 and 42 °C) to determine the effect of temperature on quenching process. The protein and NPs concentrations were 0.588 μM and 17–102 μM, respectively.

The fluorescence quenching can be quantified by the following Eq. 3:

$$Q = (F_0 - F) / F_0 \quad (\text{Eq. 3})$$

where F_0 and F are fluorescence intensities in the absence and presence of NPs, respectively³³. By assuming that the NPs–protein binding occurs at the equilibrium condition, the quenching data was fitted for Q to determine an association constant (K_a) to describe the NP–protein interaction. The association constant K is the reciprocal of the “dissociation constant”, k_D . The Stern-Volmer equation (SI: Eq. S1) is used to assess the efficiency and mechanism of fluorescence quenching. As fibrinogen potentially binds to NP surface with different domains/binding sites, exhibition of cooperativity in the binding equilibrium is expected. The binding kinetics and cooperativity in fibrinogen–zeolite interaction were determined using Hill equation (SI, Eq. S3).

Circular dichroism (CD) spectroscopy

Fibrinogen (1 mg mL⁻¹) was incubated with different zeolite concentrations (concentration range from 4.25 to 119 μM) for 1 h at 37 °C. The CD spectra of resulting solutions were recorded at the wavelengths between 190 and 260 nm with an average of 20 scans using Aviv model 215 spectropolarimeter (Lakewood, NJ, USA). All CD measurements were performed at room temperature (25 °C), in a 1 mm path cuvette. The ellipticity was represented in millidegrees.

Results and discussion

Characterization of EMT zeolite nanoparticles

Highly crystalline hexagonal EMT type zeolite NPs was synthesized and stabilized in water suspensions.^{32,34} The particle size and the morphology of NPs were determined by dynamic light scattering (DLS) and transmission electron microscopy (TEM) techniques. The EMT nanocrystals indicated unimodal particle size distribution (8–20 nm) and hexagonal morphology (SI, Figure S1a, b). The porosity of the EMT zeolite was also measured (SI, Figure S2). The EMT nanocrystals showed a combination of Types I and IV adsorption isotherm curves, indicating the presence of both micro- and textural meso- porosities (SI, Figure S2).³⁵ The size of the micropores determined using the DFT model was 0.73 nm, which is in agreement with the size of the hypocage (0.75 nm × 0.65 nm in diameter) and hypercage (0.73 nm × 0.73 nm in diameter) of the EMT-type zeolite. In addition, the size of the mesopores was 3.12 nm, which is due to the close packing of the nanoparticles resulting in textural (inter-particles) porosity. The EMT zeolite nanoparticles have a surface area of 720 m² g⁻¹, external surface area of 260 m² g⁻¹, and total pore volume of 1.32 cm³ g⁻¹. The chemical composition of the EMT zeolite was analyzed using XRF spectroscopy. The unit cell composition was Na₈₈(AlO₂)₈₈(SiO₂)₁₀₄, with the Si/Al ratio equal to 1.17, suggesting that the zeolite surface was highly negatively charged.

Hence, the high Na content was detected to counter balance the negative charge originated from the (Al–O–Si)[−] groups. The surface charge and the charge density of EMT NPs were also calculated (see Methods section). The result showed that the EMT zeolite NPs contained a surface charge of -4356 mC g^{-1} due to the high surface area and high alumina content in the framework. As a result, the high surface charge density (-6.05 mC m^{-2}) was calculated (SI, Table S1). The high surface charge and high charge density of EMT NPs are thus in line with their hydrophilic and polar nature.

Interaction of fibrinogen with EMT zeolite nanoparticles

Fluorescence spectroscopy is widely used to study the interaction of NPs and proteins³⁶. It is known that the intrinsic tryptophan (TRP) fluorescence have significant changes through protein unfolding, leading to the exposure of internal TRP that is typically hidden in the folded state³⁷. We probed fibrinogen-folding variations during the interaction with zeolite NPs using the leverage of TRP via monitoring the protein folding changes. The fluorescence spectra of fibrinogen were measured in the presence of various concentrations of EMT NPs at different temperatures (25, 37, 40 and 42 °C) (Figure 1). The maximum fluorescence peak (λ_{max}) of fibrinogens incubated with EMT NPs was observed at 342 nm, and the fluorescence intensity of fibrinogen gradually decreased as the zeolite NPs concentration increased. These results indicate that the EMT NPs, which act as a quencher, have strong interactions with the fibrinogen. In this case, one may speculate that zeolite-bounded fibrinogen may experience structural rearrangement leading to the change in microenvironment of internal TRP. Molecular interaction between protein and zeolite NPs assists to perceive the origins in addition to have safe zeolites

with more predictable biological efficacy. Therefore, several involved parameters in the fibrinogen-zeolite interaction are probed as described in the following sections.

Quenching behavior of EMT zeolite nanoparticles

It is well-recognized that NPs quench the proteins in a dynamic or static manner³⁸. Depending on the incubation temperature, the fluorophore–quencher complex is formed before (static) and/or after (dynamic) fluorophore excitation³⁹. The quenching behavior of NPs is strongly dependent on the temperature at which proteins incubate with NPs. The molecular mechanism of quenching is proposed using the Stern-Volmer equation (SI, Eq. S1). The Stern-Volmer plots and the constants of fibrinogen quenching induced by different concentrations of EMT NPs at various temperatures are shown in Figure 2 and Table 1, respectively. As can be seen, a decrease in both the Stern-Volmer quenching constants and the slope of the Stern-Volmer plot is observed at higher temperatures. This result indicates that fibrinogen is mainly quenched in a static manner. Previously, we showed that slight change in incubation temperature affects the protein decoration on the surface of NPs and consequent biological responses⁴⁰. Depending on the incubation temperature, different types and quantities of plasma proteins were adsorbed on the NPs⁶. This means that plasma proteins interact with NPs to different extent. Change in protein corona decoration is partly related to the protein conformational changes occurred at high temperature⁷. Thus, it can be suggested that newly exposed epitopes/sequences, as a result of protein unfolding, determine how proteins interact with the EMT zeolite NPs.

Binding sites of protein on EMT zeolite nanoparticles

Fibrinogen showed different orientations on the NPs surface, which is depending on the physicochemical properties of NPs (surface chemistry and size/curvature), the type of presorted

proteins and the degree of NP surface coverage^{21, 41, 42}. For example, fibrinogen tends to be adsorbed on small-sized gold (5.6–14 nm) and silica (15–60 nm) NPs *via* side-on configuration^{21, 42}. However, fibrinogen preferably attached to NPs surface through end-on configuration as the size of NPs increased⁴². The number of binding sites per protein was calculated using double-logarithm equation (Figure 3 and SI: Eq. S2)⁴³. The proteins that adopt a side-on configuration wrap the NP surface and therefore, engage more binding sites compared to the end-on state. As expected, fibrinogen, which is a hydrophilic protein, has more than one, binding sites on EMT zeolite NPs (Table 2). It is suggested that fibrinogen is mainly adsorbed on EMT NPs through side-on configuration. The influence of incubation temperature on fibrinogen-NPs interactions is presented in Figure 3. The number of binding sites per protein decreased as the incubation temperature increased from 25 to 42 °C. Thus, the temperature-induced conformational changes affect the orientation of proteins on the NPs. The proteins adopted in the side-on/end-on configuration may reorient to end-on/side-on state after structural rearrangement. Depending on the protein unfolding extent and protein orientation model, the protein-NPs interaction may form different binding strengths. Therefore, various binding energies of the interaction at different temperatures can be explained by temperature-induced conformational changes.

Cooperativity assay of fibrinogen and EMT zeolite nanoparticles

Binding kinetics and cooperativity in fibrinogen-zeolite NPs interaction were assessed using Hill equation (SI: Eq. S3). Hill coefficient determines whether different binding sites involved through protein-NP interaction are self-governed or cooperative. The calculated Hill coefficient in physiological like condition is near to 1 implying that single or multiple self-governing

binding sites mediate the fibrinogen-zeolite interaction (Figure 4) (SI: Figures S3-S5)⁴⁴. For non-cooperative protein binding, where Hill coefficient is near to 1, the affinity of proteins to NP surface is independent of the presorbed proteins. Fibrinogen has multiple domains that potentially interact with different surfaces. For example, domains D and E illustrated different affinities to the same surface⁴⁵. They also attached to zeolite NPs independently. It can be suggested that the adsorption and subsequent unfolding of each domain do not affect neighboring domain adsorption/structure.

The particle size plays crucial role in determining the cooperativity in NPs-protein interaction⁴². Considerable contradictories exist in the literatures regarding the effect of NPs size on the cooperativity in NPs-fibrinogen interaction. For example, Deng *et al.*⁴¹ showed positive cooperativity occurred when fibrinogen interacted with the gold NPs larger than 7 nm. In contrast, Lacerda *et al.*³³ demonstrated that fibrinogen preferably bound to gold NPs larger than 5 nm in a negative cooperative manner.

Analysis of thermodynamic parameters involved in the EMT zeolite nanoparticles and fibrinogen interactions

The thermodynamic parameters involved in fibrinogen-EMT NPs interaction were measured using fluorescent spectroscopy. Thermodynamic parameters such as enthalpy (ΔH), Gibbs free energy (ΔG), and entropy changes (ΔS) were indirectly calculated using the Eqs. S4 and S5 (SI) to determine the governing forces on the fibrinogen-EMT NPs interaction. The negative values for ΔG indicate that the interaction occurs spontaneously. The negative values of ΔH (-2699.05 kJ mol⁻¹) and ΔS (-787.16 J mol⁻¹ K⁻¹) imply that van der Waals forces and hydrogen bonds

mainly drive the EMT-fibrinogen interaction⁴⁶. Based on the exothermic reaction and the thermodynamic parameters obtained from van't Hoff equation and corresponded plots of fibrinogen-EMT interactions (Figure 5), it can be suggested that fibrinogen has high affinity towards EMT NPs

Secondary structure of bound fibrinogen on EMT zeolite nanoparticles

The secondary structure of fibrinogen was studied in the presence of various concentrations of EMT NPs using far-ultraviolet circular dichroism (CD) analytical approach. The CD spectra were recorded in the wavelength range 190–260 nm (SI: Figures S6-S9 and Tables S2-S11). Two negative peaks appeared at 208 nm and 222 nm are known as characteristics of typical fibrinogen structure having α -helix (Figure 6a). The reduced ellipticity at 208 nm and 222 nm indicates that the α -helix content of fibrinogen treated with NPs decreased significantly. This means that the secondary structure of fibrinogen significantly changes in the presence of EMT zeolite NPs (Figure 6b). In addition, the degree of protein denaturation gradually increased with increasing the NP concentration.

Conclusion

The structural integrity of NPs bound proteins determines the *in vivo* fate of NP and biological responses. Understanding the NPs-protein interaction is crucial for predicting the therapeutic and/or toxic impacts of NPs *in vivo*. This study revealed that the interaction between zeolite NPs and fibrinogen was strong, thermodynamically favorable and occurred in a non-cooperative

manner. The EMT zeolite NPs considerably changed the secondary structural of fibrinogen. It can be concluded that the zeolite-bound denatured fibrinogen can potentially trigger undesired biological responses *in vivo*. Therefore, the possible biological consequences resulted from zeolite-induced unfolding of proteins should be considered in future nanotoxicology studies.

Supplementary Information

Detailed results are presented in Supplementary Information.

References

1. I. Lynch and K. A. Dawson, *Nano today*, 2008, **3**, 40-47.
2. P. Aggarwal, J. B. Hall, C. B. McLeland, M. A. Dobrovolskaia and S. E. McNeil, *Advanced drug delivery reviews*, 2009, **61**, 428-437.
3. T. Cedervall, I. Lynch, S. Lindman, T. Berggård, E. Thulin, H. Nilsson, K. A. Dawson and S. Linse, *Proceedings of the National Academy of Sciences*, 2007, **104**, 2050-2055.
4. M. Mahmoudi, I. Lynch, M. R. Ejtehadi, M. P. Monopoli, F. B. Bombelli and S. Laurent, *Chemical reviews*, 2011, **111**, 5610-5637.
5. S. Tenzer, D. Docter, J. Kuharev, A. Musyanovych, V. Fetz, R. Hecht, F. Schlenk, D. Fischer, K. Kiouptsi and C. Reinhardt, *Nature nanotechnology*, 2013, **8**, 772-781.
6. M. Mahmoudi, A. M. Abdelmonem, S. Behzadi, J. H. Clement, S. Dutz, M. R. Ejtehadi, R. Hartmann, K. Kantner, U. Linne and P. Maffre, *ACS nano*, 2013, **7**, 6555-6562.
7. M. Mahmoudi, S. E. Lohse, C. J. Murphy, A. Fathizadeh, A. Montazeri and K. S. Suslick, *Nano letters*, 2013, **14**, 6-12.
8. M. J. Hajipour, S. Laurent, A. Aghaie, F. Rezaee and M. Mahmoudi, *Biomaterials Science*, 2014, **2**, 1210-1221.
9. M. J. Hajipour, J. Raheb, O. Akhavan, S. Arjmand, O. Mashinchian, M. Rahman, M. Abdolahad, V. Serpooshan, S. Laurent and M. Mahmoudi, *Nanoscale*, 2015, **7**, 8978-8994.
10. M. J. Hajipour, F. Ghasemi, H. Aghaverdi, M. Raoufi, U. Linne, F. Atyabi, I. Nabipour, M. Azhdarzadeh, H. Derakhshankhah and A. Lotfabadi, *Journal of Alzheimer's Disease*, 2017, 1-16.
11. D. Walczyk, F. B. Bombelli, M. P. Monopoli, I. Lynch and K. A. Dawson, *Journal of the American Chemical Society*, 2010, **132**, 5761-5768.
12. C. D. Walkey and W. C. Chan, *Chemical Society Reviews*, 2012, **41**, 2780-2799.
13. C. Röcker, M. Pötzl, F. Zhang, W. J. Parak and G. U. Nienhaus, *Nature nanotechnology*, 2009, **4**, 577-580.
14. Z. Bakhtiary, A. A. Saei, M. J. Hajipour, M. Raoufi, O. Vermesh and M. Mahmoudi, *Nanomedicine: Nanotechnology, Biology and Medicine*, 2016, **12**, 287-307.
15. A. M. Alkilany, N. N. Mahmoud, F. Hashemi, M. J. Hajipour, F. Farvadi and M. Mahmoudi, *Chemical research in toxicology*, 2016, **29**, 943-948.
16. M. J. Hajipour, O. Akhavan, A. Meidanchi, S. Laurent and M. Mahmoudi, *RSC Advances*, 2014, **4**, 62557-62565.
17. S. Shanehsazzadeh, A. Lahooti, M. J. Hajipour, M. Ghavami and M. Azhdarzadeh, *Colloids and Surfaces B: Biointerfaces*, 2015, **136**, 1107-1112.
18. Z. J. Deng, M. Liang, M. Monteiro, I. Toth and R. F. Minchin, *Nature nanotechnology*, 2011, **6**, 39-44.
19. M. J. Hajipour, M. R. Santoso, F. Rezaee, H. Aghaverdi, M. Mahmoudi and G. Perry, *Trends in Biotechnology*, 2017.
20. P. Roach, D. Farrar and C. C. Perry, *Journal of the American Chemical Society*, 2005, **127**, 8168-8173.
21. P. Roach, D. Farrar and C. C. Perry, *Journal of the American Chemical Society*, 2006, **128**, 3939-3945.
22. M. Mahmoudi, M. A. Shokrgozar, S. Sardari, M. K. Moghadam, H. Vali, S. Laurent and P. Stroeve, *Nanoscale*, 2011, **3**, 1127-1138.
23. C. C. Fleischer and C. K. Payne, *The Journal of Physical Chemistry B*, 2012, **116**, 8901-8907.

24. G. M. Mortimer, N. J. Butcher, A. W. Musumeci, Z. J. Deng, D. J. Martin and R. F. Minchin, *ACS nano*, 2014, **8**, 3357-3366.
25. K. Prapainop, D. P. Witter and P. Wentworth Jr, *Journal of the American Chemical Society*, 2012, **134**, 4100-4103.
26. S. W. Young, F. Qing, D. Rubin, K. J. Balkus, J. S. Engel, J. Lang, W. C. Dow, J. D. Mutch and R. A. Miller, *Journal of Magnetic Resonance Imaging*, 1995, **5**, 499-508.
27. N. Flores-López, J. Castro-Rosas, R. Ramirez-Bon, A. Mendoza-Cordova, E. Larios-Rodriguez and M. Flores-Acosta, *Journal of Molecular Structure*, 2012, **1028**, 110-115.
28. A. Tavoraro, I. I. Riccio and P. Tavoraro, *Microporous and Mesoporous Materials*, 2013, **167**, 62-70.
29. H. Derakhshankhah, M. J. Hajipour, E. Barzegari, A. Lotfabadi, M. Ferdousi, A. A. Saboury, E. P. Ng, M. Raoufi, H. Awala and S. Mintova, *ACS Applied Materials & Interfaces*, 2016, **8**, 30768-30779.
30. M. Rahimi, E.-P. Ng, K. Bakhtiari, M. Vinciguerra, H. A. Ahmad, H. Awala, S. Mintova, M. Daghighi, F. B. Rostami and M. de Vries, *Scientific reports*, 2015, **5**.
31. S. Laurent, E.-P. Ng, C. Thirifays, L. Lakiss, G.-M. Goupil, S. Mintova, C. Burtea, E. Oveisi, C. Hébert and M. De Vries, *Toxicology Research*, 2013, **2**, 270-279.
32. E.-P. Ng, D. Chateigner, T. Bein, V. Valtchev and S. Mintova, *Science*, 2012, **335**, 70-73.
33. S. H. D. P. Lacerda, J. J. Park, C. Meuse, D. Pristiniski, M. L. Becker, A. Karim and J. F. Douglas, *ACS nano*, 2009, **4**, 365-379.
34. S.-F. Wong, H. Awala. A. Vincente, R. Retoux, T.C. Ling, S. Mintova, R.R. Mukti, E.-P. Ng, *Microporous and Mesoporous Materials*, 2017, **249**, 105-110.
35. E.-P. Ng, D.T.-L. Ng, H. Awala, K.-L. Wong, S. Mintova, *Materials Letters*, 2014, **132**, 126-129.
36. Z. N. Gheshlaghi, G. H. Riazi, S. Ahmadian, M. Ghafari and R. Mahinpour, *Acta biochimica et biophysica Sinica*, 2008, **40**, 777-782.
37. J. R. Lakowicz, *Principles of fluorescence spectroscopy*, Springer Science & Business Media, 2013.
38. J. R. Lakowicz, in *Principles of fluorescence spectroscopy*, Springer, 1999, pp. 291-319.
39. G. Zhang, N. Zhao and L. Wang, *Journal of Luminescence*, 2011, **131**, 2716-2724.
40. M. Mahmoudi, M. A. Shokrgozar and S. Behzadi, *Nanoscale*, 2013, **5**, 3240-3244.
41. Z. J. Deng, M. Liang, I. Toth, M. J. Monteiro and R. F. Minchin, *ACS nano*, 2012, **6**, 8962-8969.
42. J. Deng, M. Sun, J. Zhu and C. Gao, *Nanoscale*, 2013, **5**, 8130-8137.
43. L. A. Sklar, B. S. Hudson and R. D. Simoni, *Biochemistry*, 1977, **16**, 5100-5108.
44. J. Gao, Y. Lai, C. Wu and Y. Zhao, *Nanoscale*, 2013, **5**, 8242-8248.
45. C. E. Hall and H. S. Slayter, *The Journal of Cell Biology*, 1959, **5**, 11-27.
46. Y. Mu, J. Lin and R. Liu, *Spectrochimica Acta Part A: Molecular and Biomolecular Spectroscopy*, 2011, **83**, 130-135.

Table captions

Table 1. The Stern-Volmer constants calculated for fibrinogen-EMT zeolite NPs interactions.

Table 2. Binding parameters of fibrinogen-EMT zeolite NPs interactions at different temperatures.

Table 3. Thermodynamic parameter involved in fibrinogen-EMT zeolite NPs interactions.

Figure captions

Figure 1. Fluorescence intensity of fibrinogen in the presence of different concentrations of EMT zeolite NPs at 25, 37, 40 and 42 °C.

Figure 2. The Stern-Volmer plots of fibrinogen quenching caused by different concentrations of EMT zeolite NPs at different temperatures.

Figure 3. The double-log plots $\text{Log} ((F_0 - F)/F)$ vs. Log EMT for fibrinogen-EMT zeolite NPs interactions at different temperatures.

Figure 4. The Hill plots $\text{Ln} (F_0 - F)/F)$ vs. Ln EMT for fibrinogen-EMT zeolite NPs interactions at physiological temperature (37 °C).

Figure 5. The van't Hoff plots of fibrinogen-EMT zeolite NPs interactions.

Figure 6. (a) CD spectra of fibrinogen molecules alone and in the presence of different concentrations of EMT NPs. (b) Secondary structural changes of fibrinogen in the presence of increasing concentrations of the EMT NPs. Results are mean \pm standard error of mean ($n = 20$). Star represents significant change compared to control (Fibrinogen alone) at $p < 0.05$.

Table 1.

Zeolite	T (K)	K_{sv} (M⁻¹)	K_q (M⁻¹ S⁻¹)	R²
EMT NPs	298.15	6280.4	6280.4×10 ⁸	0.97
	310.15	4532.3	4532.3×10 ⁸	0.99
	313.15	3980.3	3980.3×10 ⁸	0.99
	315.15	3611.9	3611.9×10 ⁸	0.98

Table 2.

Zeolite	T (K)	K_a (M⁻¹)	n	R²
EMT NPs	298.15	1216746.20	1.56	0.98
	310.15	15595.52	1.13	0.99
	313.15	7184.55	1.06	0.99
	315.15	3322.76	0.99	0.98

Table 3.

Zeolite	T (K)	ΔG (kJ mol⁻¹)
EMT NPs	298.15	-34.72
	310.15	-24.88
	313.15	-23.11
	315.15	-21.22

Figure 1.

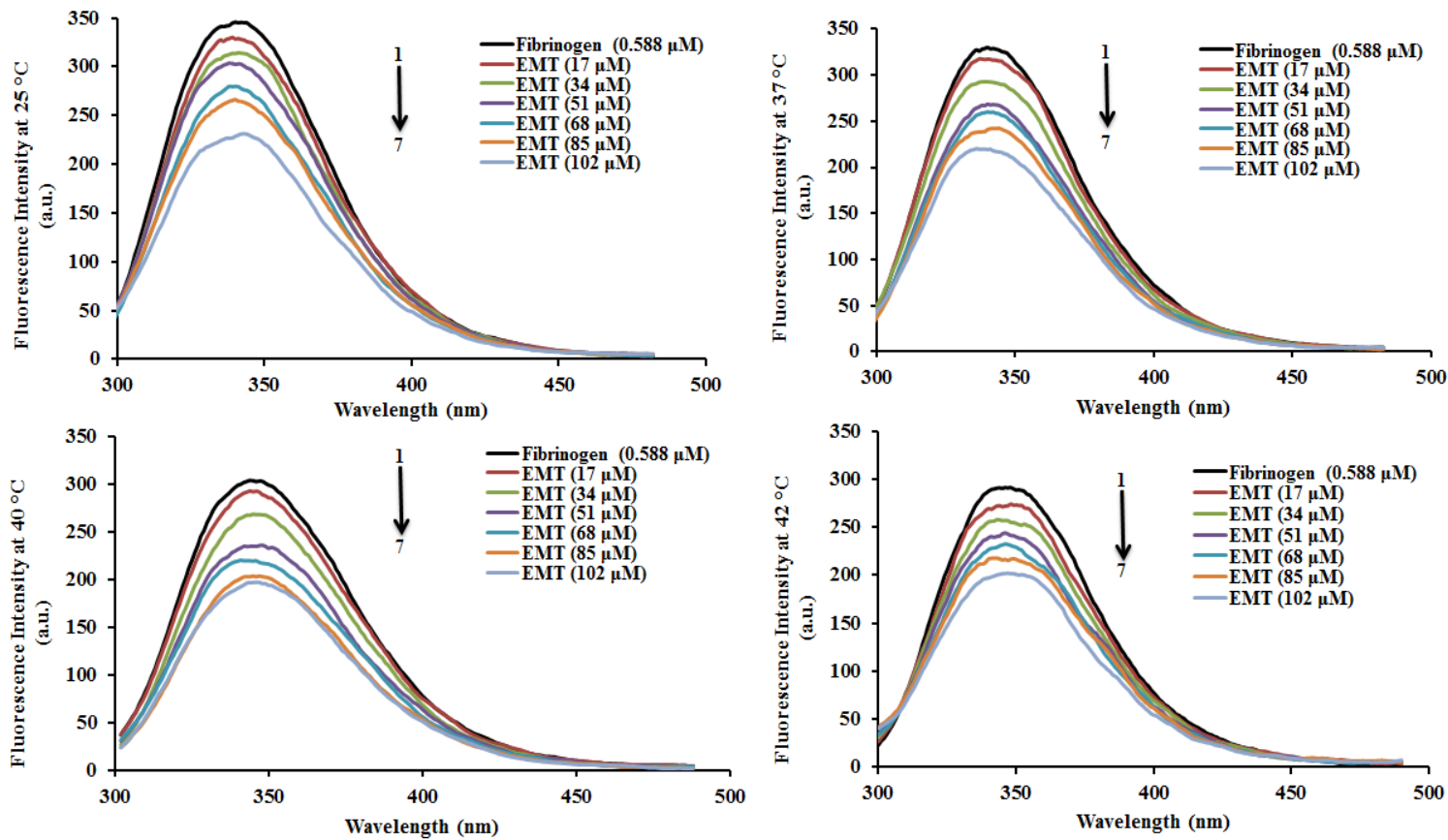


Figure 2.

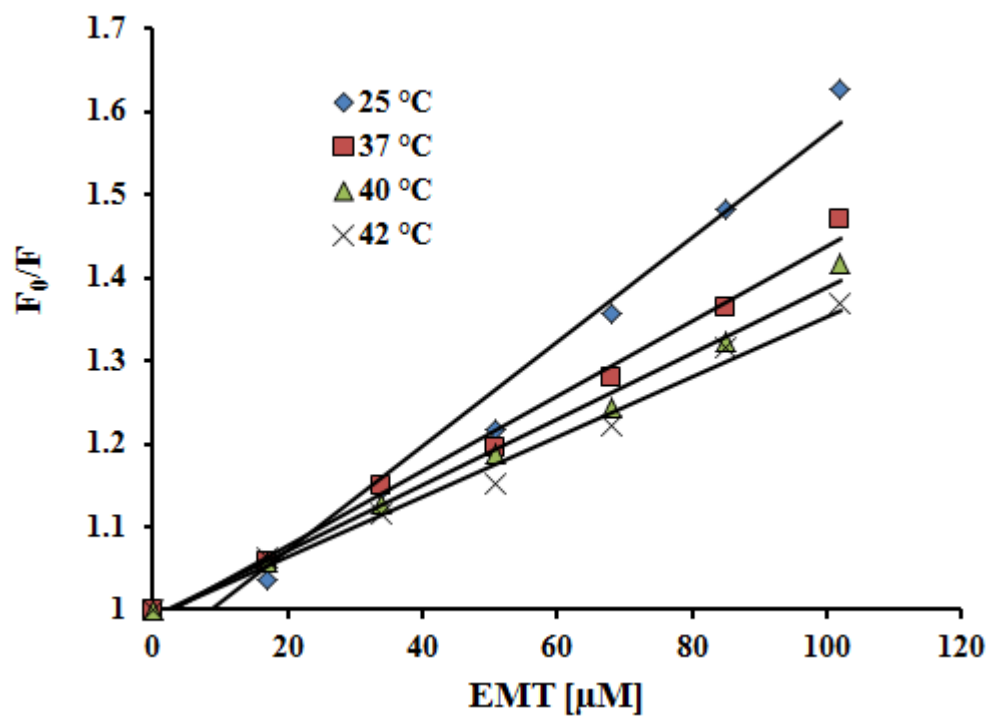


Figure 3.

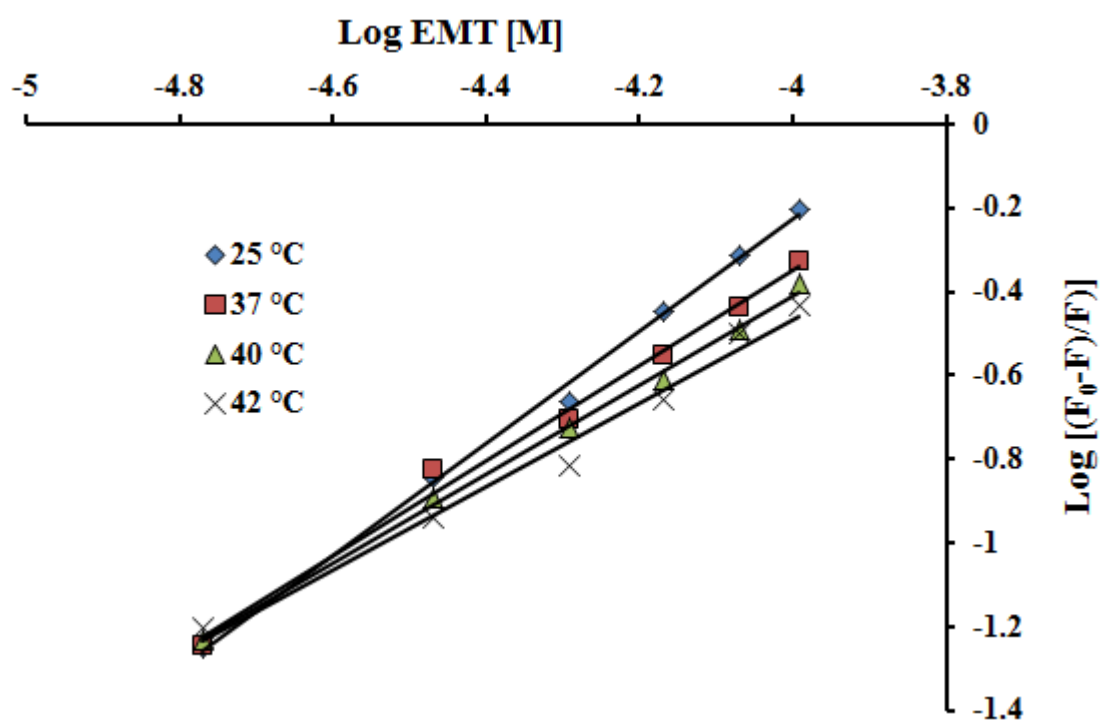


Figure 4.

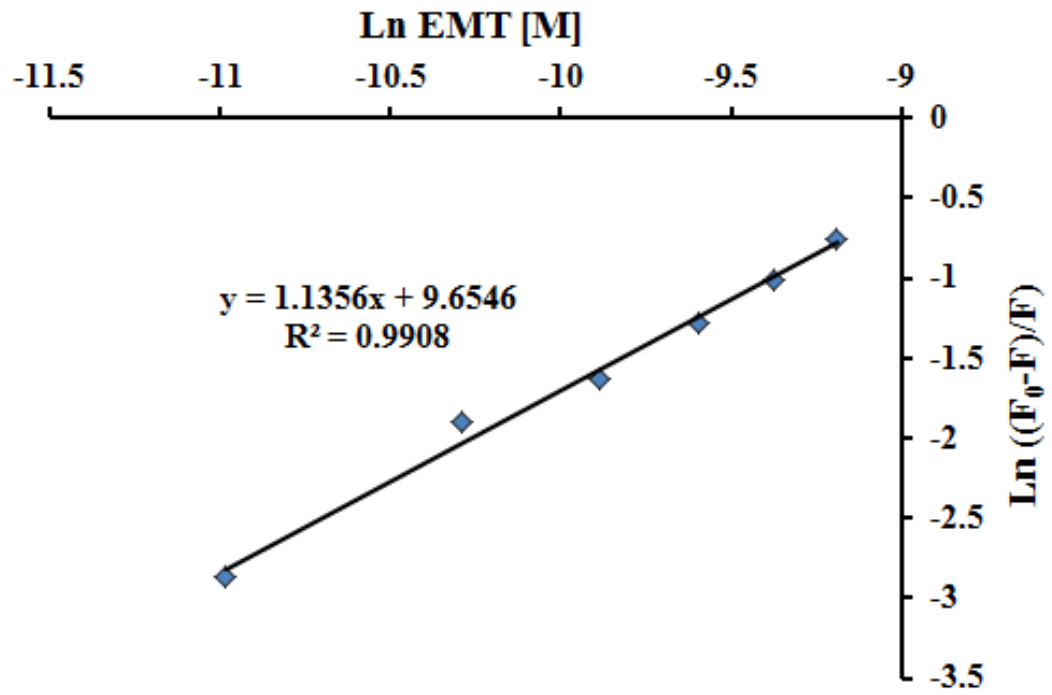


Figure 5.

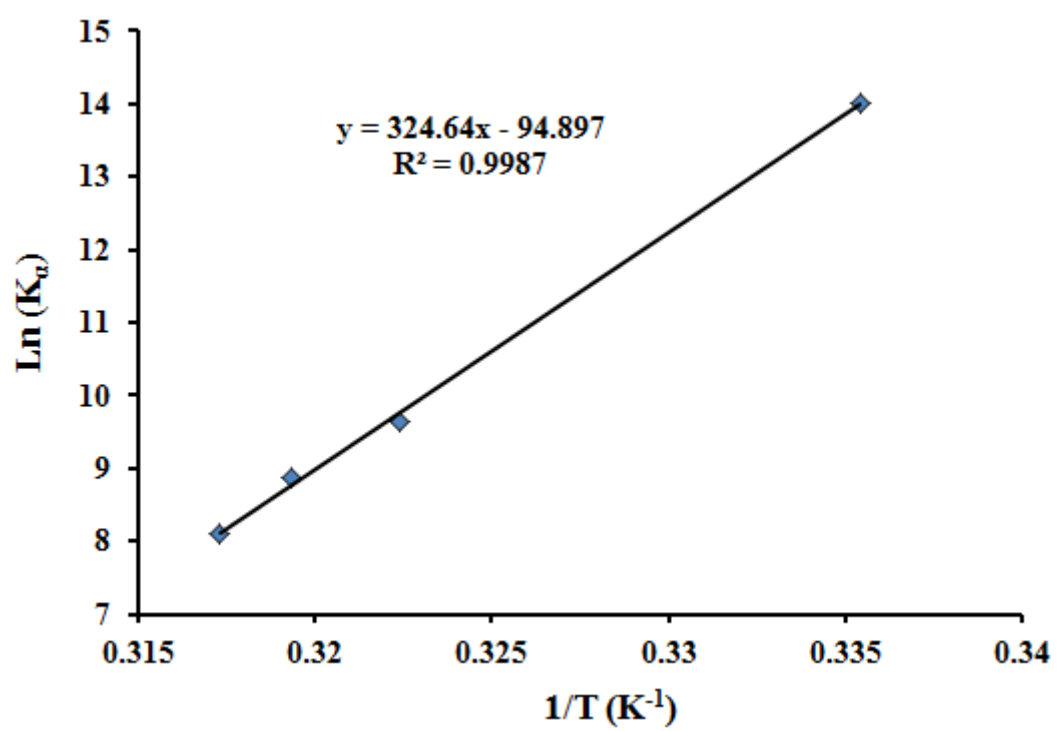
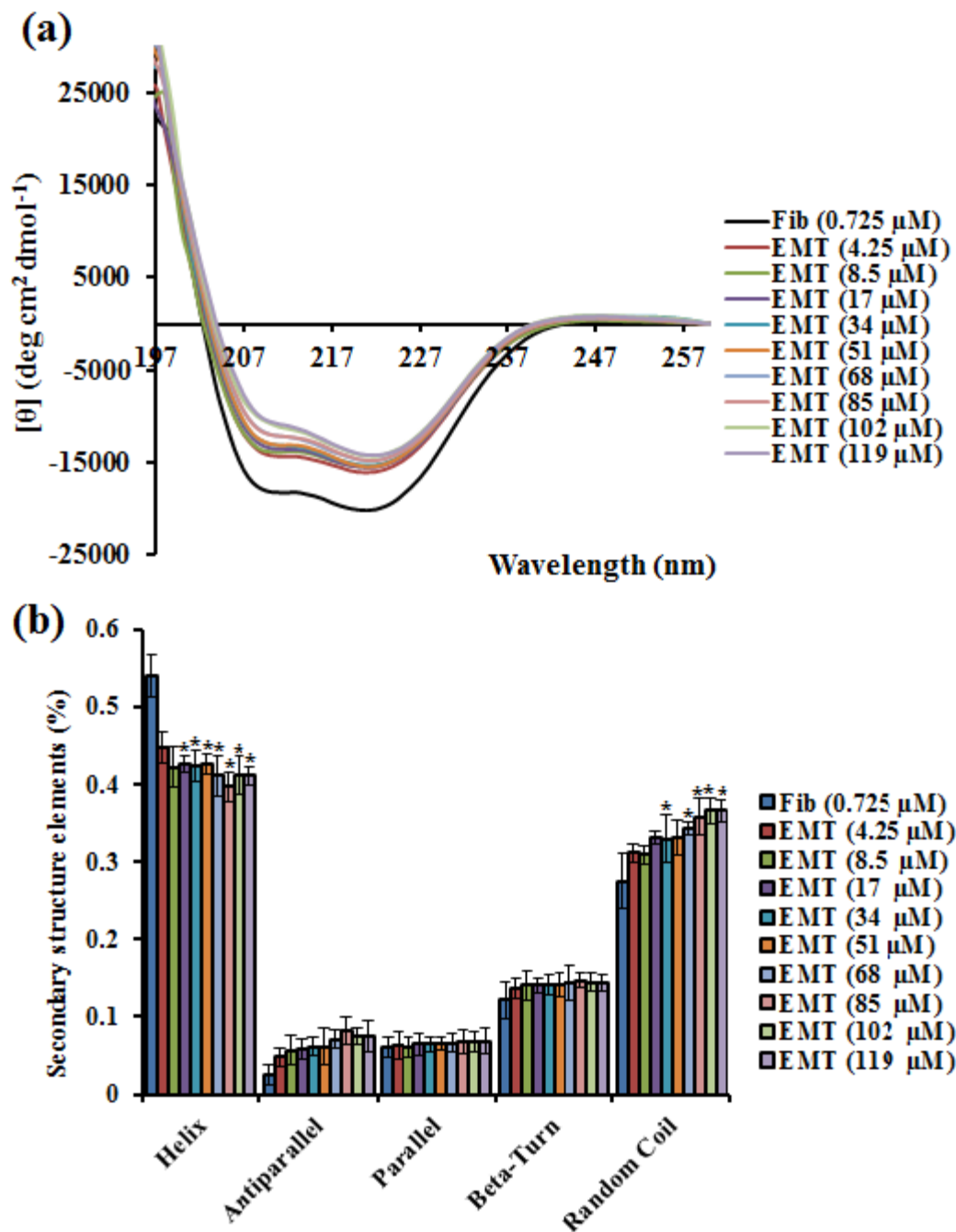


Figure 6.



Supplementray Information for

Molecular interaction of fibrinogen with zeolite nanoparticles

Hossein Derakhshankhah^{†, ‡, §, †}, Mohammad Javad Hajipour^{||, †, §}, Fereshteh Taghavi[#], Alireza Lotfabadi^{†, §, †}, Atiyeh Ghasemi[#], Ebrahim Barzegari[#], Mina Evini[#], Ali Akbar Saboury[#], Eng-Poh Ng[△], Seyed Mehdi Kamali Shahri[◆], Hussein Awala[¶], Svetlana Mintova^{¶*}, Rassoul Dinarvand^{†, §*} and Morteza Mahmoudi^{†, §, ▲*}

[†]Department of Pharmaceutical Biomaterials, Faculty of Pharmacy, [‡]Nanotechnology Research Center, Faculty of Pharmacy,

[§]Department of Pharmaceutical Nanotechnology, Faculty of Pharmacy, Tehran University of Medical Sciences, Tehran 13169-43551, Iran. [†]Department of Pharmaceutical Biomaterials, Faculty of Pharmacy, Kermanshah University of Medical Sciences, Kermanshah, Iran. ^{||}Persian Gulf Marine Biotechnology Research Center, The Persian Gulf Biomedical Sciences Research Institute, Bushehr University of Medical Sciences, Bushehr 75147, Iran.

[△]Non-Communicable Diseases Research Center, Endocrinology and Metabolism Population Sciences Institute, Tehran University of Medical Sciences, Tehran 13169-43551, Iran. [#]Institute of Biochemistry and Biophysics, University of Tehran, Tehran, Iran. [◆]Department of Chemical Engineering, The Pennsylvania State University, University Park, PA 16802, United States.

[△]School of Chemical Sciences, Universiti Sains Malaysia, 11800 USM, Malaysia.

[¶]Laboratory of Catalysis and Spectroscopy, ENSICAEN, University of Caen, CNRS, 6 Boulevard du Marechal Juin, 14050 Caen, France.

[▲]Department of Anesthesiology, Brigham and Women's Hospital, Harvard Medical School, Boston, Massachusetts 02115, United States.

* Corresponding authors: (RD) email: dinarvand@tums.ac.ir; (SM) email: mintova@ensicaen.fr; (MM) email: mmahmoudi@bwh.harvard.edu

S1. Characterization of EMT zeolites

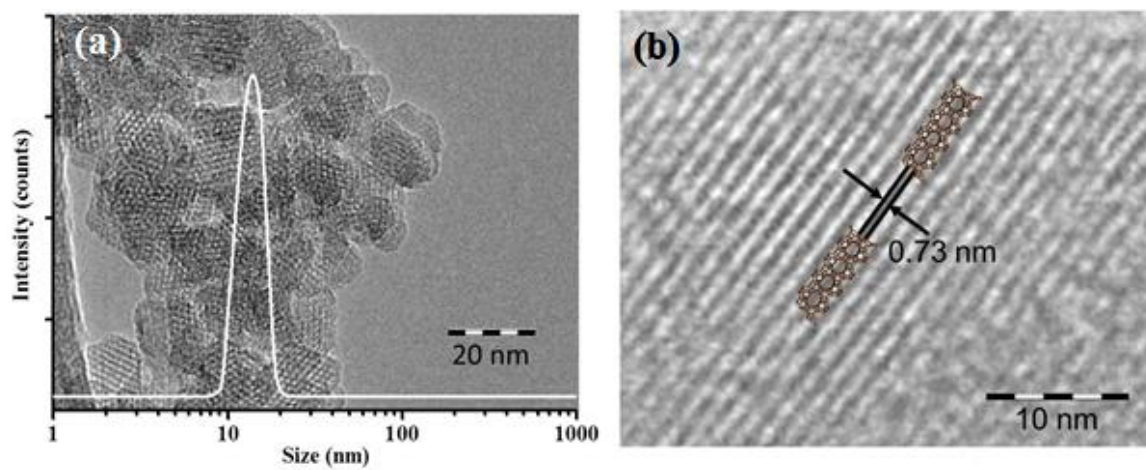


Fig S1. TEM image and DLS curve, and (b) HRTEM image of EMT zeolite nanoparticle

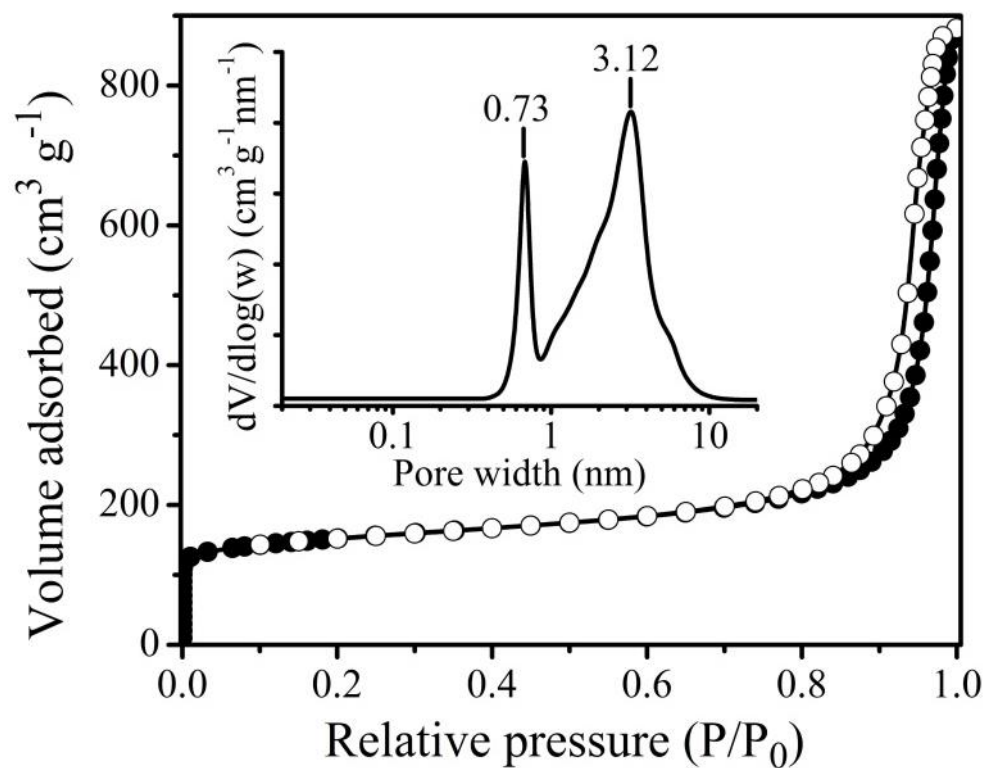


Fig S2. Nitrogen adsorption (close symbols) and desorption (open symbols) isotherms of EMT NPs. Inset: Pore size distribution derived from nitrogen sorption analysis using DFT model.

Table S1. Physicochemical characteristics of EMT zeolite NPs.

Si/Al ratio	1.17
Unit cell composition	Na ₈₈ (AlO ₂) ₈₈ (SiO ₂) ₁₀₄
S _{BET} (m ² g ⁻¹) ^a	720
S _{Ext} (m ² g ⁻¹) ^a	260
V _{micro} (cm ³ g ⁻¹) ^a	0.24
V _{meso} (cm ³ g ⁻¹) ^a	1.08
V _{Total} (cm ³ g ⁻¹) ^a	1.32
d _{micro} (nm) ^a	0.73
d _{meso} (nm) ^a	3.12
Mean particle size (nm) ^b	14.0
Charge density (mC m ⁻²) ^c	-6.05
Surface charge (mC g ⁻¹) ^d	-4.356

^aS_{BET}: BET specific surface area; S_{Ext}: external surface area; V_{micro}: micropore volume; V_{meso}: mesopore volume;

V_{total}: total pore volume; d_{micro}: micropore diameter; d_{meso}: mesopore diameter.

^bDetermined by DLS and TEM.

^cDetermined at 0.1 wt% concentration.

^dDetermined at 0.1 wt% concentration.

S2. Quenching effects of EMT NPs at different temperatures

In order to determine the molecular quenching mechanism, the fluorescence quenching results were analyzed by Stern-Volmer equation (Eq. S1).¹

$$F_0/F = 1 + K_{SV} [Q] = 1 + K_q \tau [Q] \quad (\text{Eq. S1})$$

F_0 and F reveal the fluorescence intensities at the steady-state of fibrinogen in the absence and presence of quencher (EMT-type zeolite NPs), respectively. K_{SV} is the Stern-Volmer quenching constant and it is gained from the linear regression of Stern-Volmer equation; K_q is the quenching rate constant of protein whose maximum value is known to be $2.0 \times 10^{10} \text{ L mol}^{-1} \text{ s}^{-1}$.² $[Q]$ is the concentration of quencher (EMT-type zeolite NPs). τ is the average lifetime of the fluorophore/biomacromolecule in the absence of the quencher.

The following double-logarithm equation (Eq. S2) provides more information about binding equilibrium.³

$$\text{Log} ((F_0-F)/F) = \text{Log} K + n \text{Log} [Q] \quad (\text{Eq. S2})$$

In this equation, n is the number of binding sites per protein and K is the association constant (K_a).

S3. Cooperativity studies

The Hill coefficient was measured at different temperature using Hill equation (Eq. S3) through:

$$\ln \left(\frac{F_0 - F}{F} \right) = n \ln [Q] - n \ln k_D \quad (\text{Eq. S3})$$

where F_0 and F reveal the fluorescence intensities of fibrinogen in the absence and presence of ligand (EMT-type Zeolite NPs), respectively. $[Q]$ is the concentration of ligand (EMT-type zeolite NPs). n and k_D are Hill coefficient and the protein-NP binding constant in equilibrium, respectively. With regard to the Hill equation, in the plot of $\ln \left(\frac{F_0 - F}{F} \right)$ versus $\ln [Q]$, n is the slope of the curve. The obtained plots are shown below (Figs. S3-S5):

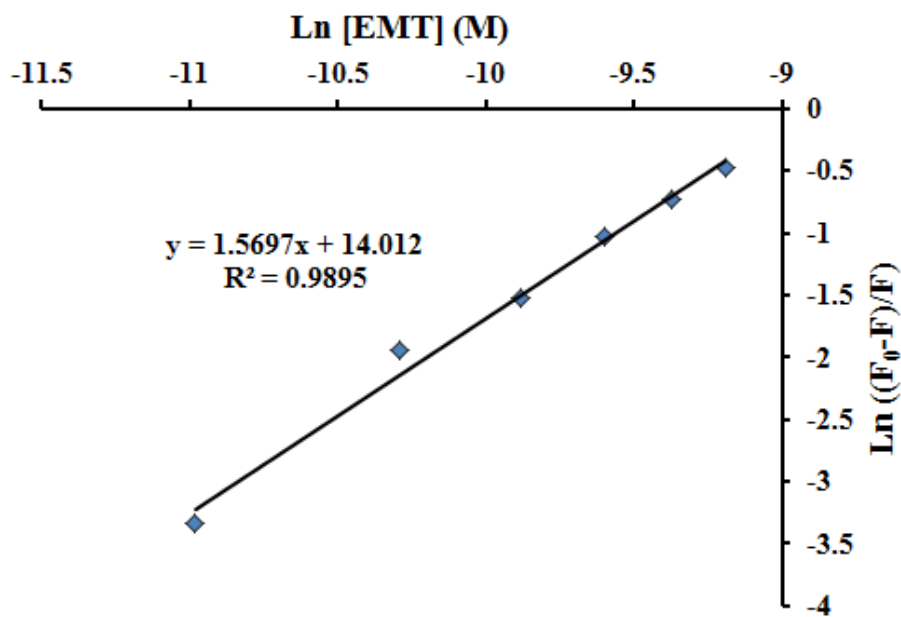
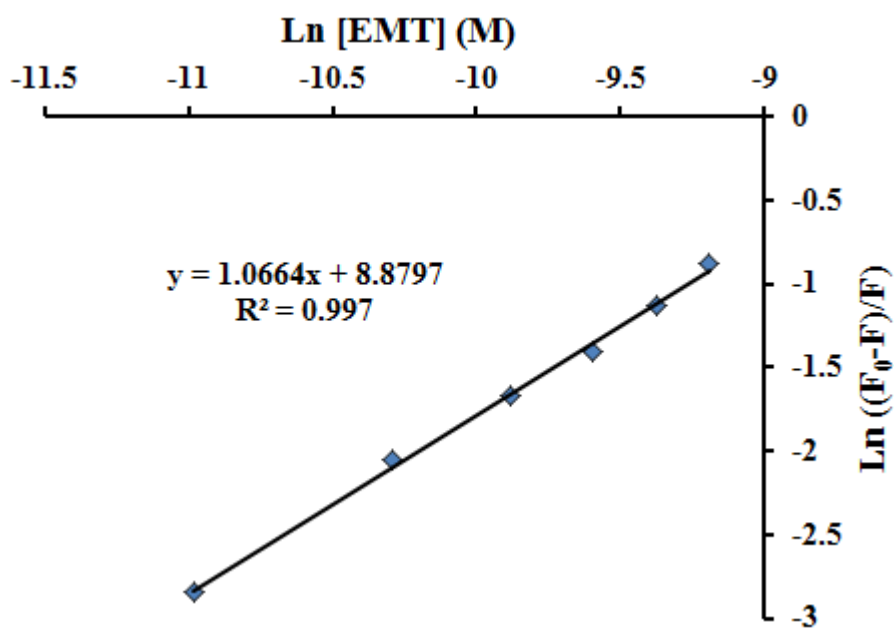


Fig.
plot of the
between
fibrinogen at



S3. Hill
interaction
EMT and
25 °C.

Fig. S4. Hill plot of the interaction between EMT and fibrinogen at 40 °C.

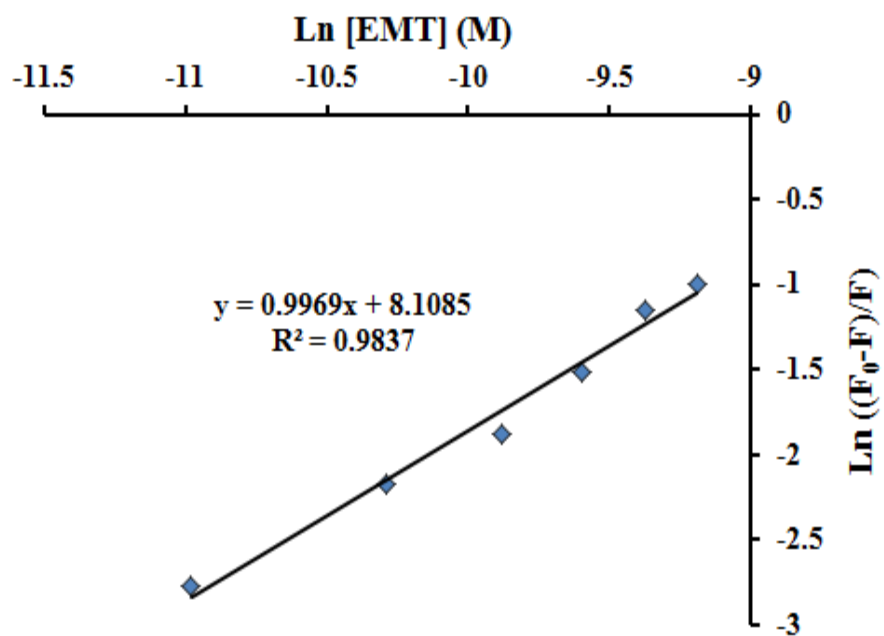


Fig. S5. Hill plot of the interaction between EMT and fibrinogen 42 °C.

S4. Thermodynamic analysis

Free energy changes of the interaction between fibrinogen and NPs were calculated using following formula:⁴

$$\Delta G = -RT\ln(K_{\alpha}) \quad (\text{Eq. S4})$$

In this equation, K_{α} is the association/binding constants for EMT NPs. T is the temperature of experiments and R is the gas constant ($8.314 \text{ J mol}^{-1} \text{ K}^{-1}$). With assuming that ΔH and ΔS values do not vary significantly over the temperature, the ΔG was calculated from Gibbs equation (Eq. S4) and other parameters can be obtained by plotting the binding constant according to van't Hoff equation (Eq. S5).⁵

$$\ln(K_{\alpha}) = -(\Delta H/RT) + (\Delta S/R) \quad (\text{Eq. S5})$$

S5. Circular Dichroism data

Tables S2–S11 and Figures S6–S9 give the detailed information obtained from the CD spectroscopy on the interreaction between fibrinogen and EMT zeolite NPs.

Table S2. Percentage of different secondary structures in fibrinogen (0.25 mg mL^{-1}).

195-260 200-260 205-260 210-260

	nm	nm	nm	nm
Helix	48.00%	56.30%	55.40%	56.30%
Antiparallel	3.50%	2.10%	2.20%	2.30%
Parallel	6.80%	6.20%	5.80%	5.80%
Beta-Turn	13.00%	11.80%	11.80%	12.20%
Random Coil	29.50%	26.10%	26.80%	27.60%
Total Sum	100.70%	102.40%	102.00%	104.10%

Table S3. Percentage of different secondary structures in fibrinogen treated with EMT (25 $\mu\text{g mL}^{-1}$).

	195-260 nm	200-260 nm	205-260 nm	210-260 nm
Helix	42.80%	45.50%	45.00%	45.30%
Antiparallel	5.60%	4.40%	4.50%	4.60%
Parallel	6.90%	6.40%	6.00%	5.90%
Beta-Turn	14.10%	13.30%	13.30%	13.90%
Random Coil	30.40%	31.20%	31.30%	31.50%
Total Sum	99.90%	100.80%	100.10%	101.20%

Table S4. Percentage of different secondary structures in fibrinogen treated with EMT (50 $\mu\text{g mL}^{-1}$).

	195-260 nm	200-260 nm	205-260 nm	210-260 nm
Helix	37.80%	43.70%	43.40%	44.00%
Antiparallel	7.90%	4.80%	4.90%	5.00%
Parallel	6.60%	6.30%	5.90%	5.80%
Beta-Turn	15.10%	13.60%	13.60%	14.10%
Random Coil	29.70%	31.30%	31.10%	31.40%
Total Sum	97.10%	99.70%	98.90%	100.30%

Table S5. Percentage of different secondary structures in fibrinogen treated with EMT (100 $\mu\text{g mL}^{-1}$).

	195-260	200-260	205-260	210-260
--	---------	---------	---------	---------

	nm	nm	nm	nm
Helix	41.50%	43.80%	42.40%	42.50%
Antiparallel	7.00%	5.30%	5.60%	5.80%
Parallel	7.20%	6.60%	6.10%	6.00%
Beta-Turn	14.40%	13.60%	13.70%	14.50%
Random Coil	31.30%	33.10%	34.10%	33.90%
Total Sum	101.40%	102.40%	101.80%	102.70%

Table S6. Percentage of different secondary structures in fibrinogen treated with EMT (200 $\mu\text{g mL}^{-1}$).

	195-260 nm	200-260 nm	205-260 nm	210-260 nm
Helix	41.80%	43.40%	42.10%	42.10%
Antiparallel	7.50%	5.50%	5.70%	6.00%
Parallel	7.10%	6.70%	6.10%	6.00%
Beta-Turn	14.70%	13.60%	13.70%	14.60%
Random Coil	29.00%	33.80%	34.60%	34.30%
Total Sum	100.10%	103.00%	102.20%	103.00%

Table S7. Percentage of different secondary structures in fibrinogen treated with EMT (300 $\mu\text{g mL}^{-1}$).

	195-260 nm	200-260 nm	205-260 nm	210-260 nm
Helix	44.50%	43.30%	41.60%	41.40%
Antiparallel	6.70%	5.60%	6.00%	6.40%
Parallel	7.20%	6.80%	6.20%	6.00%
Beta-Turn	14.50%	13.60%	13.80%	14.70%
Random Coil	28.10%	34.20%	35.30%	35.00%
Total Sum	100.80%	103.60%	102.80%	103.50%

Table S8. Percentage of different secondary structures in fibrinogen treated with EMT (400 $\mu\text{g mL}^{-1}$).

	195-260	200-260	205-260	210-260
--	---------	---------	---------	---------

	nm	nm	nm	nm
Helix	42.50%	42.20%	40.20%	39.60%
Antiparallel	8.00%	6.30%	6.70%	7.20%
Parallel	7.30%	6.90%	6.20%	6.00%
Beta-Turn	14.80%	13.80%	14.00%	15.10%
Random Coil	29.10%	35.50%	36.80%	36.10%
Total Sum	101.70%	104.70%	103.90%	104.00%

Table S9. Percentage of different secondary structures in fibrinogen treated with EMT (500 $\mu\text{g mL}^{-1}$).

	195-260 nm	200-260 nm	205-260 nm	210-260 nm
Helix	39.10%	41.50%	39.50%	38.50%
Antiparallel	10.60%	6.90%	7.20%	8.00%
Parallel	7.40%	7.10%	6.40%	6.10%
Beta-Turn	15.40%	13.90%	14.10%	15.30%
Random Coil	29.90%	37.10%	38.60%	37.40%
Total Sum	102.50%	106.50%	105.80%	105.30%

Table S10. Percentage of different secondary structures in fibrinogen treated with EMT (600 $\mu\text{g mL}^{-1}$).

	195-260 nm	200-260 nm	205-260 nm	210-260 nm
Helix	45.60%	41.40%	39.50%	38.10%
Antiparallel	7.20%	7.10%	7.40%	8.30%
Parallel	7.70%	7.20%	6.40%	6.10%
Beta-Turn	14.30%	13.90%	14.00%	15.40%
Random Coil	30.20%	38.20%	39.70%	38.10%
Total Sum	105.00%	107.90%	107.00%	106.10%

Table S11. Percentage of different secondary structures in fibrinogen treated with EMT (700 $\mu\text{g mL}^{-1}$).

	195-260	200-260	205-260	210-260
--	---------	---------	---------	---------

	nm	nm	nm	nm
Helix	45.60%	41.40%	39.50%	38.10%
Antiparallel	7.20%	7.10%	7.40%	8.30%
Parallel	7.70%	7.20%	6.40%	6.10%
Beta-Turn	14.30%	13.90%	14.00%	15.40%
Random Coil	30.20%	38.20%	39.70%	38.10%
Total Sum	105.00%	107.90%	107.00%	106.10%

Alterations of different secondary structure types by increasing the EMT concentrations ($\mu\text{g mL}^{-1}$), studied at various wavelength ranges, have been depicted in Figures S6–S9. Results are mean \pm standard error of mean ($n = 20$). Asterisk means significant change compared to control (fibrinogen alone) at $p < 0.05$.

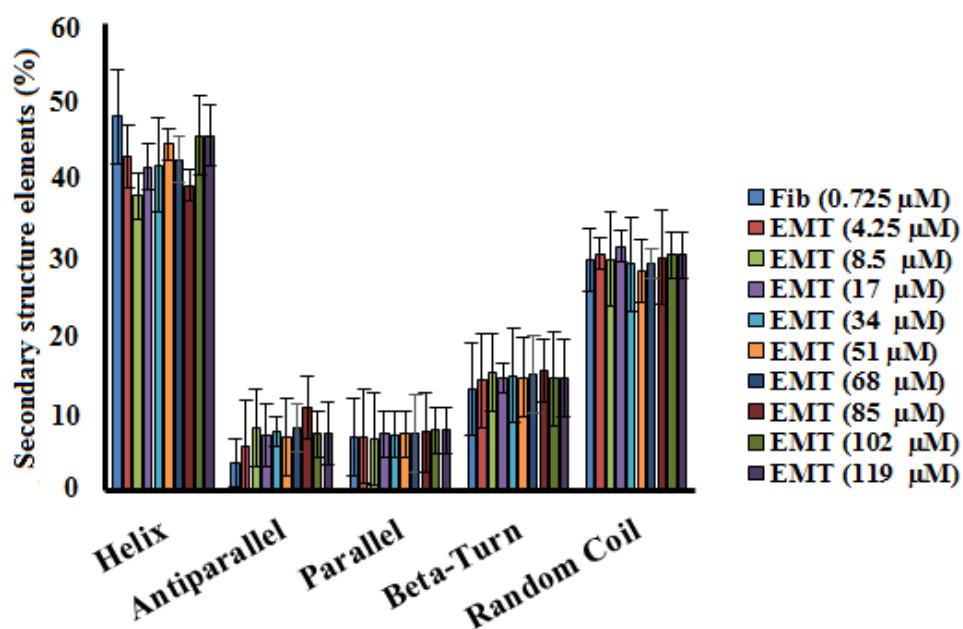


Fig. S6 Fibrinogen secondary structure content changes upon binding EMT studied at 195–260 nm.

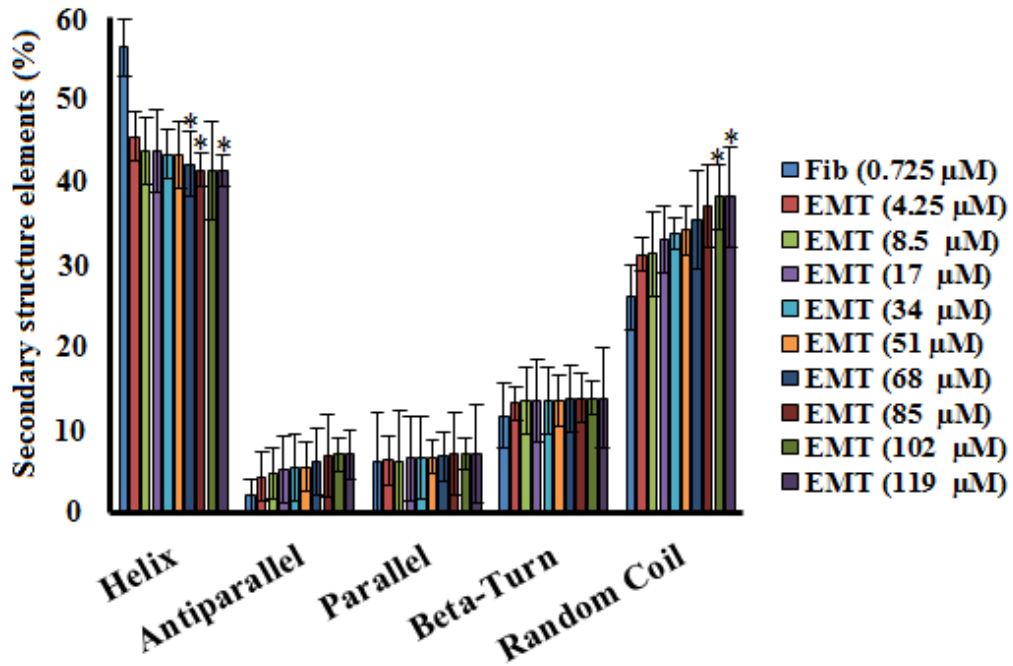


Fig. S7 Fibrinogen secondary structure content changes upon binding EMT studied at 200–260 nm.

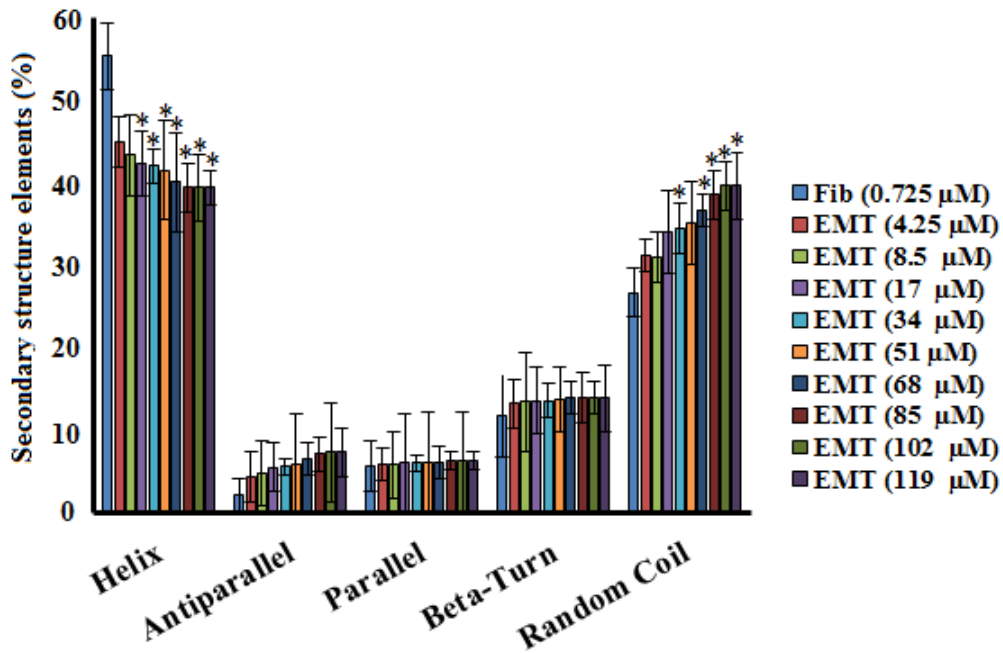


Fig. S8 Fibrinogen secondary structure content changes upon binding EMT studied at 205–260 nm.

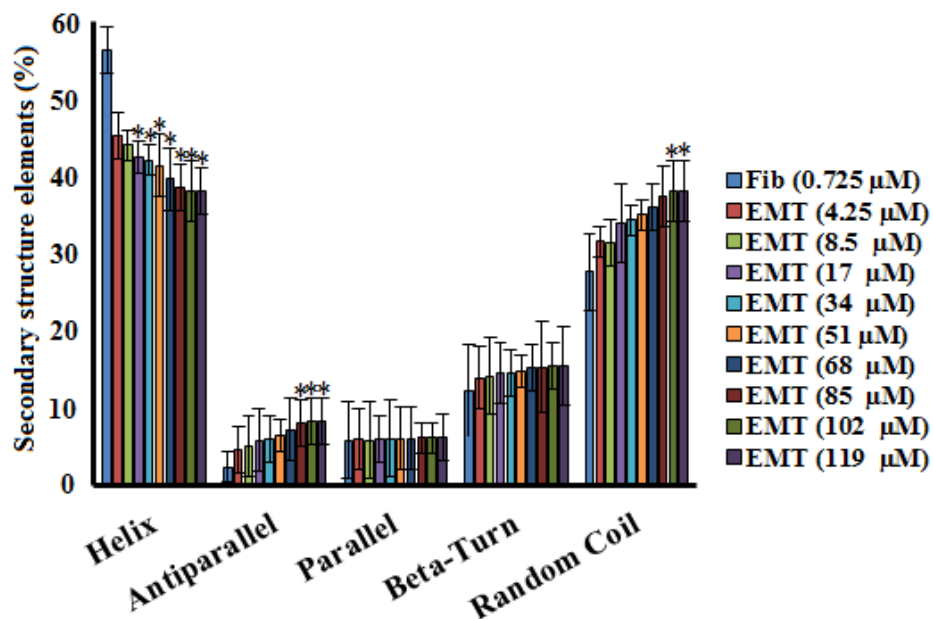


Fig. S9 Fibrinogen secondary structure content changes upon binding EMT studied at 210–260 nm.

References

1. Zhou, Q.; Xiang, J.; Tang, Y.; Liao, J.; Yu, C.; Zhang, H.; Li, L.; Yang, Y.; Xu, G., Investigation on the interaction between a heterocyclic aminal derivative, SBDC, and human serum albumin. *Colloids and Surfaces B: Biointerfaces* 2008, *61* (1), 75-80.
2. Gerbanowski, A.; Malabat, C.; Rabiller, C.; Gueguen, J., Grafting of aliphatic and aromatic probes on rapeseed 2S and 12S proteins: influence on their structural and physicochemical properties. *Journal of agricultural and food chemistry* 1999, *47* (12), 5218-5226.
3. Sklar, L. A.; Hudson, B. S.; Simoni, R. D., Conjugated polyene fatty acids as fluorescent probes: binding to bovine serum albumin. *Biochemistry* 1977, *16* (23), 5100-5108.
4. Ross, P. D.; Subramanian, S., Thermodynamics of protein association reactions: forces contributing to stability. *Biochemistry* 1981, *20* (11), 3096-3102.
5. Zhang, Z.; Tang, R., Synthesis and fluorescence properties of Tb (III) complex with a novel β -diketone ligand as well as spectroscopic studies on the interaction between Tb (III) complex and bovine serum albumin. *Journal of Molecular Structure* 2012, *1010*, 116-122.